Materials Horizons

ROYAL SOCIETY OF CHEMISTRY

COMMUNICATION

View Article Online
View Journal

Cite this: DOI: 10.1039/d5mh02106e

Received 5th November 2025,
Accepted 21st November 2025

DOI: 10.1039/d5mh02106e

rsc.li/materials-horizons

Towards nickel–titanium shape memory alloys for coatingless icephobic materials

Luca Stendardo, [ab] Francesca Villa, [b] Davide Parlato, [a] Riccardo Motto, [a] Mauro Mameli, [c] Carlo Antonini *[a] and Paola Bassani *[b]

To mitigate the effects of icing in industry and everyday life, significant efforts have been directed in the last decade towards the development of surfaces with low ice adhesion. Although several materials have emerged as potential candidates for the development of ultra-low ice adhesion coatings, most of them lack mechanical durability, as they are susceptible to abrasion. The present study explores the ice adhesion properties of a nickel–titanium (NiTi) shape memory alloy (SMA), which combines a relatively low elastic modulus and mechanical durability, revealing that SMAs can display icephobic properties, with ice adhesion strength down to 100 kPa, comparable to that of soft polymers. NiTi samples of varying thicknesses are characterized for their critical shear stress and interfacial toughness, highlighting the significance of sample thickness and stiffness in ice adhesion characterization. Additionally, the impact of surface roughness on ice adhesion is examined. As a metallic material, NiTi offers superior mechanical durability, opening up a novel route for durable, coatingless technologies against ice adhesion.

New concepts

This study introduces a nickel–titanium shape memory alloy as a durable, coatingless material with remarkably low ice adhesion, achieving adhesion strengths below 100 kPa, typically seen only with organic coatings or on soft polymers. While traditional materials generally suffer from durability issues against mechanical abrasion, NiTi as a metallic material offers resistance to erosion and abrasion similar to titanium alloys, known for their excellent strength. This study demonstrates that, on tuning the substrate thickness, NiTi shows an exceptionally low interfacial toughness and excellent ice removal capabilities, outperforming those of conventional low-strength materials. Additionally, under low temperature conditions typical of icing conditions, the elastic modulus of NiTi significantly decreases, further reducing the interfacial toughness and enhancing its ice removal efficiency. This effect is generally not observed in structural metals such as aluminum or titanium. As such, we define a new class of icephobic materials, suggesting that thin, coatingless metallic plates could enable novel designs for ice protection systems, eliminating the need for surface coatings susceptible to degradation.

1 Introduction

Unwanted ice accretion on exposed industrial structures and facilities poses a significant threat, endangering both infrastructure and human life. In the aeronautics industry, ice build-up can have catastrophic outcomes, including the limitation of aircraft maneuverability and aerodynamic efficiency. Conventional active de-icing techniques, such as thermal and chemical de-icing, have shown inherent limitations regarding energy efficiency and environmental compatibility.[1–5] Consequently, over the past two decades, research on passive surfaces with icephobic properties has flourished due to their potential to reduce the energy consumption of de-icing systems and to increase operational safety.[1,6–8]

Although icephobic surfaces working under all conditions are yet to be developed, low elastic modulus (or simply, soft) materials are emerging, as they have shown exceptionally low ice adhesion due to their ability to form stress concentrations at the ice–substrate interface.[9–11] Soft icephobic surfaces are typically polymers, which can be precisely tuned to obtain the desired properties and to minimize the adhesion to ice. However, they are susceptible to mechanical abrasion and erosion, which limits their durability.

In this context, several research groups have directed their efforts towards developing durable metallic alloys with low ice adhesion properties, such as superhydrophobic coatings on aluminum alloys.[4,12–14] Superhydrophobic surfaces have shown exceptionally low ice adhesion values under low humidity conditions. The air voids within the superhydrophobic microstructure can effectively reduce the pinning of drops to the

[a] Department of Materials Science, University of Milano – Bicocca, Milano, Italy. E-mail: carlo.antonini@unimib.it
[b] National Research Council of Italy, Institute of Condensed Matter Chemistry and Technologies for Energy, CNR ICMATE, Unit of Lecco, Via Previati 1/E, 23900 Lecco, Italy. E-mail: paola.bassani@cnr.it
[c] Department of Energy Systems Territory and Constructions (DESTEC) Largo L. Lazzarino 2, 56121 Pisa, Italy

substrate and allow for effective shedding of the water before freezing occurs.[15–17] However, under high humidity conditions, which are common under extreme icing conditions, ice nucleation and freezing might still occur. The condensation and water intrusion into the microstructures cause mechanical interlocking between the ice and the substrate, leading to increased ice adhesion.[18–21] Also, such superhydrophobic coating-based surfaces suffer from durability issues, due to mechanical abrasion, which can be particularly severe due to rain and sand erosion.

The possibility of designing and fabricating metallic icephobic surfaces, which do not rely on short-lasting coatings or surface treatments, is still an open challenge. Integrating icephobic bulk features into metallic materials could dramatically improve the industrial application of such low ice adhesion surfaces.

For this reason, a thorough understanding of the ice adhesion mechanism is essential to develop novel, more efficient, and reliable surfaces. According to the current knowledge, fracture at the ice–substrate interface can generally be described in terms of adhesion strength and bonding energy (or, more precisely, interfacial toughness).[22–24] A stress-dominated interfacial fracture is manifested by an instantaneous rupture along the entire interface, whereas a toughness-dominated fracture is characterized by crack propagation along the interface. Recently, materials with low interfacial toughness showed high ice removing capability, surpassing the performance of conventional low strength materials,[25–27] demonstrating that effective control of the fracture mechanism at the interface can potentially lead to innovative solutions against icing. Therefore, the characterization of potential icephobic materials should include the measurement of both the adhesion strength and the interfacial toughness, especially in the case of metals.

Among metallic materials, shape memory alloys (SMAs) are functional materials that can be of interest for icephobicity; differently from purely structural materials such as aluminum or steel, they are known for their peculiar mechanical properties (superelasticity and shape memory effect (SME)[28]) that make them valuable in various industrial applications. For instance, in the biomedical field, SMAs are widely utilized as stent materials and orthopedic implants, and in cardiovascular or neurological surgeries,[29,30] mostly relying on superelasticity. In robotics, the SME is exploited for actuators in robotic hands and wearable devices. Advances over the past two decades have significantly improved the material design and fabrication technologies of SMAs. This progress has enabled the development of small-scale actuators with complex designs.[31–35] Additionally, SMAs are widely employed in the automotive and aeronautics industries.[36,37]

The first studies analyzing the ice adhesion properties of SMAs are starting to emerge. A recent example is the study of Dubey,[38] where a Cu-based SMA was deposited on steel substrates by thermal spray coating to measure its ice adhesion strength. The author was able to effectively reduce the ice adhesion strength compared to that of other commercially available spray coatings. However, even though the coating exhibited a phase transition around the icing temperature (0 °C), the effect of this phase change on ice adhesion was not directly investigated.

In the context of aircraft de-icing, the SME has been implemented as an active strategy to mechanically modify the outer wing surface and to induce ice removal by surface bending or shearing.[39,40] In these systems, nickel–titanium (NiTi) SMAs, commonly known as nitinol, are used as an outer skin to the wing area, and active actuation of the SMAs along the shear plane (*i.e.* straining) induces a shedding of the ice mass. Therefore, ice is detached from the NiTi skin due to a shear motion of the ice–substrate interface.

Nonetheless, ice adhesion on NiTi has not yet been systematically characterized and hence the intrinsic passive icephobic potential of NiTi SMAs has been so far overlooked. By understanding the passive de-icing capabilities of the material, the morphological and mechanical properties of NiTi SMAs can be optimized, ultimately leading to more efficient NiTi-based de-icing systems. In this study, we present an in-depth characterization of ice adhesion on NiTi alloy substrates and demonstrate that SMAs inherently display icephobic properties, facilitating passive surface de-icing.

To this end, critical shear stress and interfacial toughness were measured on NiTi samples of varying thicknesses, highlighting the importance of material thickness and sample stiffness in ice adhesion characterization. Additionally, the effect of surface roughness on NiTi ice adhesion was examined by comparing samples with different mechanical surface treatments. It should be noted that the NiTi samples used in this study did not undergo martensitic phase transformation within the tested temperature range. This selection was deliberate, enabling isolated analysis of how mechanical stiffness (determined by specimen thickness) and surface roughness affect ice adhesion.

The results demonstrate that, depending on the substrate thickness and surface finish, NiTi can achieve ice adhesion values comparable to those of soft PDMS, a material widely known for its extremely low ice adhesion. Unlike PDMS, however, NiTi is a metallic material and provides superior mechanical durability, making it a promising candidate for the development of novel de-icing technologies based on shape memory alloys, possibly also exploiting martensitic phase transitions.

2 Results and discussion

2.1 Comparative ice adhesion study

The ice adhesion properties of various NiTi samples, each with a thickness of 0.2 mm and different surface morphologies, were compared in this study (see Section 4.1 for material specifications).

In this phase, ice adhesion was assessed using the standard push-off method, which involves measuring the average ice adhesion strength. This was determined by calculating the ratio of the force required to detach the ice to the interface area (F/A). As mentioned in Section 2.3, selected samples were used for a more in-depth characterization of ice adhesion on NiTi, focusing on the distinction between stress- and toughness-

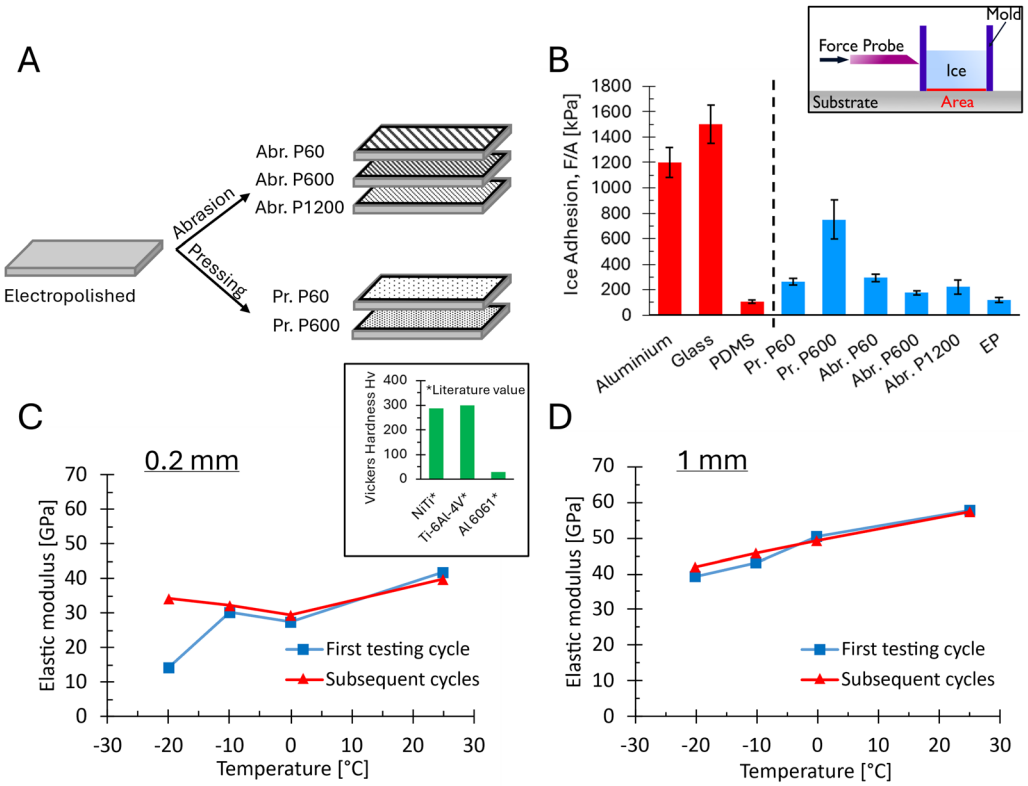

Fig. 1 (A) Schematic diagram of the sample preparation methods. (B) Ice adhesion results on abraded (Abr.), pressed (Pr.), and electropolished (EP) samples. For Abr. and Pr., the sandpaper grit size is indicated. Ice adhesion values for aluminum, glass, and PDMS obtained using the exact same ice adhesion test system (schematic diagram is provided in the inset) and with the same test parameters are reported for comparison.[11,41–43] (C) Elastic moduli of the raw material used for the preparation of the samples with 0.2 mm and (D) 1 mm thickness, respectively. The moduli have been obtained by performing uniaxial tensile tests on dog-bone specimens. Each test was repeated 3 times, and first cycle *vs.* subsequent cycles results are reported. Standard deviations for the average values of the subsequent cycles are less than 1%. For comparison, the elastic modulus of Al 6061 is 68 GPa, while that of Ti–6Al–4V is in the range of 104 to 113 GPa.[44] Inset in (C): Vickers hardness (H_V) values of NiTi,[45] Ti–6Al–4V,[46] and Al 6061.[47]

dominated fracture mechanisms.[25,41] Additionally, Section 2.4 presents a detailed examination of how surface morphology affects ice adhesion on NiTi.

The samples were initially subjected to electropolishing, a process that involved the removal of surface oxides and impurities resulting from the fabrication procedure. Various roughness features, with R_a in the range of 0.40–3.39 μm, were then created using SiC polishing paper by pressing (samples Pr. P60 and P600) or abrading (samples Abr. P60, P600, and P1200), where P60, P600, and P1200 indicate the granulometric size of the paper used (Fig. 1A).

Afterwards, samples with different roughness features and morphologies were tested for their ice adhesion (measured as force over area, *F*/*A*, see the inset of Fig. 1B) according to the protocol defined in Section 4.4 (Fig. 1B, blue). For comparison, the ice adhesion values for aluminum, glass, and polydimethylsiloxane (PDMS) obtained using the exact same test system and with the same testing parameters are reported as well. Since these reference data have been previously published in earlier studies,[11,41–43] they are visually distinguished and displayed in red in Fig. 1B.

A remarkable result is the low ice adhesion value of only 118 ± 22 kPa observed for the electropolished (EP) sample. To put this into perspective, the same ice adhesion test system with the same test protocol was also used to test the adhesion of ice to soft polymers, specifically PDMS, and the results are reported in the work of Ospina *et al.*[43] In their study, it was shown that for the same ice column shape (8 mm diameter), the ice adhesion values on PDMS vary between 70 and 140 kPa, depending on the degree of lubrication of the polymer. PDMS is generally known to be a promising low ice adhesion material, and several references are available highlighting its remarkable performance against icing.[11,48–50]

PDMS exhibits low ice adhesion due to the elastic modulus mismatch between PDMS and ice, where PDMS undergoes deformation under applied loads, thereby promoting ice release. The modulus mismatch promotes ice removal when substrates possess lower moduli than that of ice. Also, lubrication by uncrosslinked chains can play an important role.[43] Note that the reverse scenario, due to high-modulus materials, does not necessarily yield the same beneficial effect, as demonstrated by the elevated adhesion commonly seen with high-modulus metals like steel or titanium.

The ice adhesion value obtained for the EP NiTi sample was in the same range as that obtained for PDMS, even though the elastic modulus of NiTi is about 4 orders of magnitude higher

than that of PDMS and about 3 to 5 times higher than that of glaze ice. Being a metallic material, NiTi naturally exhibits better mechanical durability[45,51] (see also inset of Fig. 1C) and opens up the way for novel coating-free technologies against ice adhesion based on NiTi SMA.

A potential explanation for such low force-to-area (F/A) values could be the occurrence of different fracture mechanisms, specifically stress- or toughness-dominated fractures. Previous studies have demonstrated that buckling of metallic plates can significantly reduce the adhesion of ice on thin metallic substrates.[52] However, a comprehensive investigation into the effect of substrate thickness on adhesion strength and interfacial toughness is yet to be conducted. In Section 2.3, the effects of substrate thickness on the transition between fracture mechanisms are analyzed.

2.2 Measurement of the elastic modulus of the NiTi samples

The effect of substrate thickness on the interfacial fracture mechanism was studied on two NiTi samples with thicknesses of 0.2 mm and 1 mm. Both substrates were superficially abraded using 1200 grit SiC polishing paper, as this surface treatment resulted in the lowest surface roughness. The surface roughness values are R_a = 0.40 ± 0.15 μm and R_a = 0.48 ± 0.03 μm, respectively (see Section S1 in the SI for the full roughness characterization using an optical 3D profilometer). Thus, given the similar roughness values, it was possible to isolate the effect of substrate thickness on ice adhesion. To verify that both substrates interact similarly with water, the quasi-static water contact angle was measured. Both the advancing contact angle (98° ± 1° *vs.* 103° ± 1°) and the receding contact angle (51° ± 3° and 63° ± 4° for 0.2 mm and 1 mm thicknesses, respectively) were comparable (see Section S2 in the SI).

The elastic modulus of NiTi is known to change with temperature and metal-working processes.[44] The rolling process used to achieve different material thicknesses, such as 0.2 mm and 1 mm, typically introduces varying degrees of cold deformation. Therefore, the elastic moduli of the NiTi alloys used in this study were determined through tensile tests conducted at different temperatures. The results are presented in Fig. 1C and D (see also Section S3 in the SI for stress–strain graphs).

Unlike common structural metals such as aluminum or titanium, it can be noticed that the elastic modulus of the NiTi substrates was generally lower at lower temperatures, particularly during the first testing cycles. For instance, at −20 °C and for the sample with a thickness of 0.2 mm, the elastic modulus was below 15 GPa, which is approximately one order of magnitude lower than that of the Ti-6Al-4V titanium alloy.[53] It is worth noting that the Vickers hardness (H_V) of NiTi[45] is practically identical to that of the titanium alloy[46] (see the inset of Fig. 1C), suggesting exceptional durability despite lower elastic modulus.

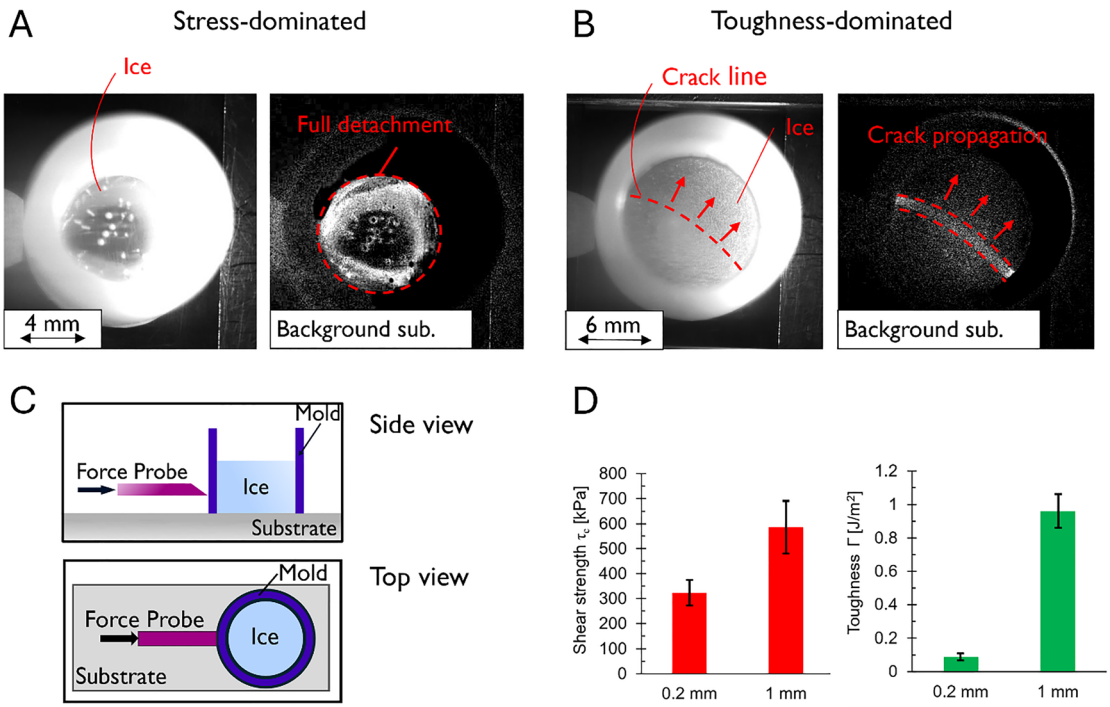

Fig. 2 (A) High speed visualization of a stress-dominated, instantaneous detachment of ice without any visible crack propagation. The background subtraction highlights the entire interface, and the whole detachment process takes less than 0.17 ms. (B) Toughness-dominated detachment with clearly visible crack propagation. In this case, the whole detachment process takes approximately 2.8 ms. (C) Side view and top view schematic diagrams of the experimental ice adhesion measurement setup. (D) Numerically derived shear strength and toughness values of the NiTi samples with thicknesses of 0.2 and 1 mm, respectively. The values have been determined by using the SSIFs and TPs, after measuring experimentally the force required to detach the ice in a stress- or toughness-dominated mode.

2.3 Fracture mechanism analysis

Interfacial fractures can occur instantaneously (stress-dominated) or gradually (toughness-dominated) (see Fig. 2A and B). In the case of instantaneous detachment, the process is governed by critical stress, *i.e.*, the minimum stress value along the ice–substrate interface. Conversely, gradual detachment is controlled by interfacial toughness, defined as the critical strain energy release rate at the interface.[22,23] The complete theoretical framework used to describe and characterize the interface fracture events follows the theories proposed by Martin *et al.* and Leguillon[22,23] and is proposed in Section S4 in the SI.

Traditional methods of ice adhesion characterization do not differentiate between these fracture mechanisms. Typically, the adhesion strength is calculated as the force-to-area ratio (F/A), regardless of the mechanism involved. However, in this work, both interfacial ice adhesion strength and toughness were measured using the testing framework developed by Stendardo *et al.*[41,54]

The ice adhesion tests were carried out using the horizontal shear test device introduced in previous studies[11,41,43,54] (see schematic diagrams in Fig. 2C and details in Section 4.4) and by strategically changing the ice block shape to trigger either of the fracture mechanisms (stress- or toughness-dominated). For both cases, the force required to detach the ice block was measured experimentally. Then, the critical stress (τ_c) and toughness (Γ) values were calculated with the help of numerically derived correction factors.[41,54] These correction factors take the geometry of the test system (the force application height and the shape of the ice block) and the force required to detach the ice as inputs and give τ_c and Γ as outputs. The experiments were performed in a series, with variations in the test system geometry to alternately trigger stress- or toughness-dominated fracture mechanisms.

Recalling an earlier study,[54] the two correction factors for τ_c and Γ, the shear stress intensity factor (SSIF) and the toughness parameter (TP) respectively, are defined as shown in eqn (1) and (2).

$$\mathrm{SSIF} = \frac{F/A}{\tau_c} \tag{1}$$

$$\mathrm{TP} = \frac{\Gamma D^3}{F^2} E_{\mathrm{ice}} \tag{2}$$

The left-hand sides of eqn (1) and (2) are numerical constants, specific to the ice adhesion test system geometry. The right-hand sides comprise the variables to be calculated numerically (τ_c and Γ) and other variables that are known experimentally, such as the ice removal force F, the ice–substrate interface area A, the ice block diameter D, and the elastic modulus of the ice sample E_{ice}. Further details on the numerical model used to obtain these correction factors can be found in Section 4.5.

For the horizontal push test used in this study and for cylindrical ice samples, the SSIFs and TPs were previously calculated in the study of Stendardo *et al.*[54] for a substrate elastic modulus above 35 GPa. Based on the tensile test results shown in Fig. 1C (at −10 °C), the 1 mm samples exhibited an elastic modulus greater than 35 GPa, so the correction factors calculated in ref. 54 were directly used. Differently, the 0.2 mm samples showed an elastic modulus below 35 GPa, so new correction factors for stress- and toughness-dominated ice detachment were calculated by numerical modeling. The elastic modulus and thickness of the materials were adopted in the numerical model described in Section 4.5, and simulations were performed for the 0.2 mm substrates to find new SSIF and TP.

The adopted SSIFs and TPs used for the calculation of the true critical shear stress and toughness of the substrates are summarized in Table 1.

After determining the SSIFs and the TPs for the different test system geometries, the force required to detach the ice was measured experimentally for each sample and for each fracture mechanism (see SI Section S5). The so resulting true shear strength and toughness are reported in Fig. 2D. It can be seen that the difference between shear strengths (323 kPa *vs.* 585 kPa) was less pronounced than the difference between the toughness values (0.09 J m^{-2} *vs.* 0.97 J m^{-2}). Therefore, the thickness of the substrate has a major influence on the toughness of the interface, with low substrate thicknesses favoring toughness-dominated detachments.

Adhesion and fracture mechanisms between two solid bodies at an interface depend on the entire system, not solely the interface properties. Thinner metallic plates, on which the ice is grown, are more prone to bending under load. Although this bending does not alter the interface, it concentrates the elastic strain energy at the interface, weakening the interface bond. This process results in crack-opening displacements that facilitate ice detachment, even under low loads. Consequently, the interface toughness, or resistance to crack propagation, is significantly reduced. Specifically, decreasing the substrate thickness from 1 mm to 0.2 mm reduces the toughness by approximately an order of magnitude.

The reduction in toughness with decreasing thickness of the metallic plates is a general substrate mechanical effect that is not exclusive to NiTi. However, the extent of this effect is larger on NiTi substrates – especially at low temperatures typical of de-icing applications – compared to other high-modulus metals, such as aluminum or titanium.

Table 1 Geometrical parameters and correction factors (SSIF and TP) used for the calculation of the true critical shear stress and toughness of the NiTi substrates of 0.2 and 1 mm thickness, respectively

Diameter [mm]	Ice height H [mm]	Pushing height h [mm]	SSIF	TP
NiTi (0.2 mm thickness)				
8	6	1	1.9	—
12	3	1	—	2.2
NiTi (1 mm thickness)				
8	6	1	2.1	—
12	1.5	1	—	3.5

To demonstrate this, additional ice adhesion tests were performed on aluminum and titanium substrates with thicknesses of 0.2 mm and 1 mm. The substrates were polished superficially using grit-1200 SiC paper to achieve a similar surface roughness to the NiTi substrates. Fig. 3A and B present the toughness values for the 0.2 mm and 1 mm samples, respectively.

The toughness values on the 1 mm samples are in the range of 0.5–1 J m^{-2}, which is commonly reported in the literature for both aluminum and titanium substrates.[55–57] Generally, the standard deviations of these measurements are also high, reaching values of up to 50% of the mean. In our experiments with 1 mm substrates, NiTi exhibited the highest toughness, followed by aluminum and titanium.

Moving to the 0.2 mm substrates, data show that all three samples exhibit reduced toughness compared to their 1 mm counterparts due to the aforementioned mechanical effect. However, the NiTi sample exhibits the most significant reduction in toughness. This can be explained by the fact that structural metals, such as aluminum or titanium, typically have a constant or slightly increasing elastic modulus at lower temperatures. In contrast, NiTi shows a reduction in elastic modulus at lower temperatures. These unique mechanical properties may enhance bending under load at low temperatures, facilitating ice detachment from thin sheet systems.

In this study, the effects of the elastic modulus and substrate thickness were analyzed using substrates that did not undergo martensitic phase transitions at the testing temperatures. Therefore, even without the heat effect associated with martensitic transformations, using NiTi substrates for low-toughness surfaces offers a significant advantage due to their mechanical properties at low temperatures. Future research will build on this preliminary analysis to further investigate the de-icing potential of SMAs that undergo phase transformation.

The results reported above highlight the importance of distinguishing between fracture regimes for accurate understanding and replication of ice adhesion results. This differentiation is crucial for the design of icephobic coatings and materials.

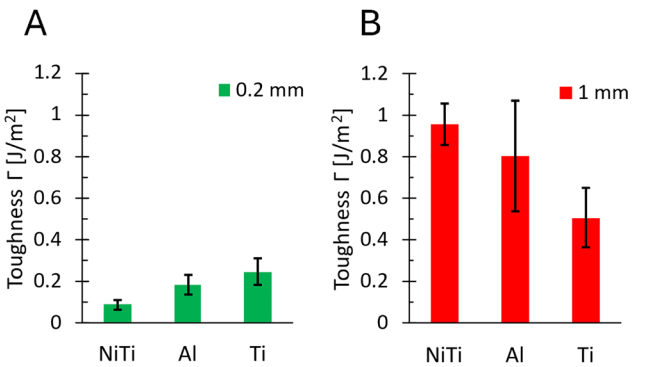

Fig. 3 Toughness values for NiTi, Al, and Ti substrates with thicknesses of (A) 0.2 mm and (B) 1 mm.

2.4 Roughness effects on NiTi ice adhesion

The roughness of the samples tested in Section 2.1 was evaluated using a 3D optical profilometer ("R_a 3D" and "S_a 3D") and a 2D stylus profilometer ("R_a 2D") (see Fig. 4A and B and Section 4.2 for specifications and details). Fig. 4A and B display the correlation between such values. Static water contact angles (Fig. 4C) and ice adhesion (Fig. 4D) were measured on all the samples and plotted against R_a 2D. Additionally, 3D optical microscope images and extended roughness profiles of all the samples used in this section are provided in Section S1 of the SI.

The results from both profilometers indicate that the observed morphological differences are at least partially captured by the two roughness measurement methods. Similar trends in relative sample roughness are evident, with Pr. P60 and Abr. P60 exhibiting a higher roughness compared to Abr. P600, Abr. P1200, and EP. However, relying on a single measurement method can be misleading for characterizing surface roughness. For instance, the mean roughness of the Pr. P600 sample was similar to that of the Abr. P60 sample when measured using a 2D stylus profilometer (1.25 ± 0.20 μm and 1.21 ± 0.18 μm, respectively). Yet, the same Pr. P600 sample exhibited a threefold lower average roughness when measured using a 3D optical profilometer (Fig. 4A and B). To show the qualitative difference in the distribution of asperities and valleys between the Pr. P600 and Abr. P60 surfaces, and for better interpretation of the roughness measurements, SEM images are provided in Fig. 4E and F (additional SEM images of all the samples are provided in Section S7 of the SI).

Fig. 4D shows how the ice adhesion strength cannot be directly correlated simply with the average roughness values. While it is generally accepted that increased surface roughness can result in increased mechanical interlocking of the ice, leading to higher ice adhesion strengths, a direct correlation between these values remains elusive.[20,58,59]

The average roughness of the Pr. P600 sample and that of the Abr. P60 sample measured using a 2D stylus profilometer were practically identical (1.25 ± 0.20 μm and 1.21 ± 0.18 μm, respectively), as discussed previously. However, the ice adhesion value of the Abr. P60 sample is still 2.5 times lower than that of the Pr. P600 sample.

Comparing the samples Abr. P600 and Pr. P60, the ice adhesion values were 177 ± 17 kPa and 296 ± 15 kPa, respectively. The R_a 2D roughness value, however, differs by a factor of 7.0 with values of 0.48 ± 0.12 μm and 3.39 ± 0.66 μm, respectively.

Our data demonstrate a lack of one-to-one correlation between ice adhesion value and any of the considered roughness parameters (see the SI, Section S6). This example also shows that mechanical interlocking effects cannot be described only by an average roughness value. Indeed, it was previously shown by Vercillo *et al.*[60] that the influence of the spatial period and specific shape of the microstructure can have an effect on ice adhesion (see also Fig. 4E and F). It can be hypothesized that the size and the distribution of the surface features

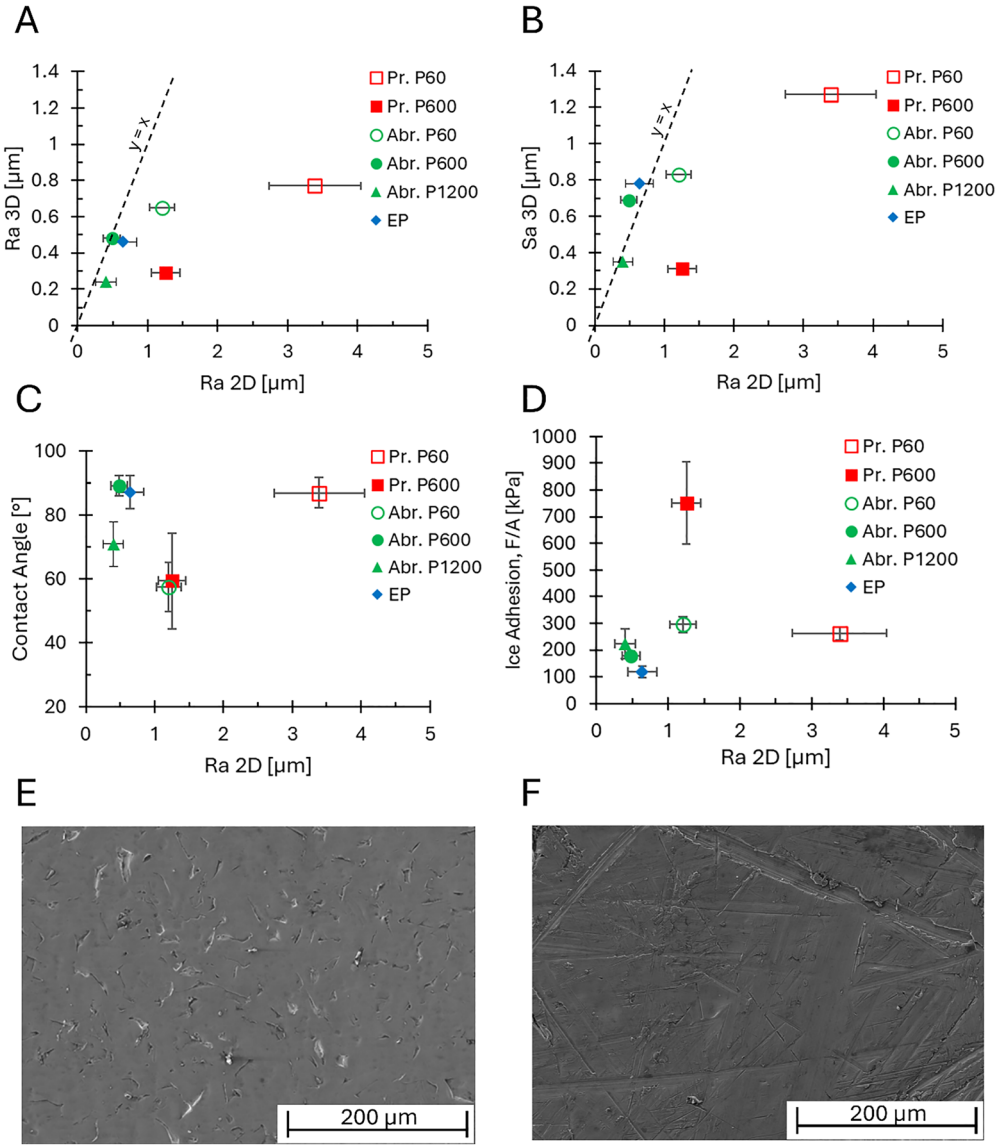

Fig. 4 (A) Average roughness values (R_a) obtained using a 3D optical profilometer on a line profile and using a 2D stylus profilometer. (B) Average surface roughness values (S_a 3D) against average profile roughness values (R_a 2D) obtained using 3D optical and 2D stylus profilometers, respectively. (C) Contact angle *versus* R_a 2D values. (D) Ice adhesion (F/A) *versus* R_a 2D values. The SEM images of (E) the "Pr. P600" sample and (F) the "Abr. P60" sample.

influence the stress distribution and, therefore, the crack propagation behavior at the ice–substrate interface. Small-scale surface features increase ice adhesion due to a substantial increase in the effective surface area, resulting in effective interlocking of the ice at the interface.[61] Conversely, larger surface features, while not increasing the effective surface area to the same extent, can act as stress concentration points, introducing interface discontinuities that act as crack initiation sites, therefore reducing the resulting ice adhesion.[11,62,63]

A clear example of this behavior can be observed in the Pr. P60 and Pr. P600 samples (see Section S7 of the SI for SEM images). Pr. P60 exhibited a lower ice adhesion than Pr. P600, with values of 262 ± 25 kPa and 750 ± 155 kPa, respectively. The distance between the surface features for these samples was 340 ± 90 µm for Pr. P60 and 28 ± 7 µm for Pr. P600. Similarly, the feature sizes were 219 ± 38 µm for Pr. P60 and 19 ± 4 µm for Pr. P600 (see the SI, Section S8). Larger features with greater spatial periods resulted in lower ice adhesion compared to smaller features with smaller spatial periods.

3 Conclusions

Nickel–titanium (NiTi) was evaluated for its ice adhesion properties, revealing its potential as a novel coatingless icephobic material. We found that, depending on the surface finish and substrate thickness, NiTi can achieve ice adhesion values comparable to those of soft PDMS, which is renowned for its extremely low ice adhesion. As a metallic material, NiTi offers superior mechanical durability, paving the way for novel de-icing technologies based on NiTi SMAs.

Also, decreasing the substrate thickness from 1 mm to 0.2 mm leads to a reduction of the shear strength by approximately a factor of 2 and a decrease in interfacial toughness by more than one order of magnitude. This finding highlights that adhesion and fracture mechanisms are influenced by the entire system, not just the interface properties. Thinner metallic plates are more prone to bending under applied loads, consequently reducing the toughness of the interface, even when the surface roughness remains constant.

The low ice adhesion properties of the materials presented in this study are not achieved through an ultra-low elastic modulus, such as that of PDMS, nor through micro-/nanostructuring of the surface, as with superhydrophobic surfaces. Differently, it is achieved by controlling the ice–substrate fracture mechanisms and optimizing the substrate thickness. Further analysis on thin metallic plates for de-icing applications could enable the design of effective and durable materials, defining a new class of icephobic surfaces.

The study confirmed that an increased surface roughness can lead to increased mechanical interlocking of ice, resulting in higher ice adhesion strength. However, no direct correlation was found between ice adhesion strength and any of the roughness parameters. This result suggests that mechanical interlocking effects cannot be described only by average roughness values but are likely influenced by the spatial period and specific shape of the microstructure.

The NiTi samples employed in this study did not exhibit martensitic phase transitions in the temperature range corresponding to icing conditions. This choice was made to independently investigate the effects of mechanical stiffness (determined by sample thickness) and roughness on ice adhesion. Future research could involve SMAs with martensitic phase transition within the temperature range of the ice adhesion tests to analyze the impact of these transitions on ice adhesion properties.

4 Materials and methods

4.1 Material specifications

NiTi superelastic lab grade plates with a nominal composition of Ni-50.8%/Ti-49.2% were used to prepare the samples used in this study. The samples are coatingless, *i.e.*, they are self-standing samples entirely composed of NiTi. The composition used exhibits superelastic behavior and possesses martensitic phase transformation temperatures below ambient temperatures. The materials used to prepare the 0.2 mm thickness and 1 mm thickness samples were characterized by DSC analysis (TA Instruments DCS C100), provided in Section S9 of the SI.

The DSC characterization revealed differences in the transformation curves between the two sample thicknesses. While the thickness itself does not directly influence the position and shape of the transformation peaks, the different cold-working procedures required to obtain samples of different thicknesses resulted in varying levels of constraints for the martensitic transformation. It is important to notice, however, that for both the 1 mm and 0.2 mm samples, no transformation peaks were observed in the temperature range where the ice adhesion tests were performed (−10 to −15 °C). The martensitic phase change has therefore no effect on the thermodynamic properties of the samples.

4.2 Roughness measurements

A 2D stylus profilometer (Mitutoyo® Surftest SV-500 with a tip radius of 2.5 μm) was used to measure the average R_a values on a profile length of 12.5 mm. At least three measurements were performed on each sample.

The 3D optical roughness measurements were carried out using a Keyence VHX-X1 digital optical microscope. The lenses used were VHX-E20 and VHX-E100. The average R_a values were calculated on a profile length of 3 mm, while the S_a values were calculated over an area of 3 mm × 3 mm.

4.3 Contact angle measurements

The wettability of the surfaces was characterized *via* static and quasi-static contact angle measurements by the sessile drop method using an in-house instrument. Water droplets up to 8 μL volume were deposited gently and vertically under atmospheric conditions at room temperature in all measurements. Contact angle measurements were conducted using both the free software ImageJ (https://imagej.net) and the open-source software tool "Dropen".[64]

4.4 Ice adhesion measurements

The adhesion of ice to the different NiTi substrates was assessed using a custom horizontal shear test, detailed in ref. 11 and 41. This method involves placing a hollow cylinder (nylon, PA.6) with 8 mm or 12 mm internal diameter over the sample and filling it with distilled water. The height of the water column varied depending on the fracture mechanism that was to be triggered (see Table 1). The sample was then cooled to −10 °C using a Peltier plate beneath the sample holder, while maintaining relative humidity below 2%. The cooling system was housed within an environmental chamber, which was supplied with a continuous flow of nitrogen gas (ambient temperature T_{amb} = 20 °C). Once the water was completely frozen (the conditioning time was kept between 15 and 20 minutes), a commercial force sensor (Mark-10, Force Gauge M5-20) was used to apply pressure to the cylinder with a metallic tip at a height of 1 mm from the surface, moving at 0.01 mm s^{-1} until the ice fully detached.

4.5 Numerical simulation methods

Finite element analysis (FEA) in Ansys Mechanical 2022 R1 was used to calculate interface stresses and strain energy in the ice adhesion test setup. The numerical model employed in this study was similar to the one used in ref. 54 and it replicated the key components of the ice adhesion test, which included the ice column, nylon mold, and NiTi substrate. The model geometry matched the experimental setup and the force was modeled as a distributed pressure over a 1 × 1 mm^2 area on the outside of the mold, corresponding to the contact area with the force probe in the experimental setup. The contact conditions

between ice and the substrate were set to ''bonded'', while a frictionless condition was used between the mold and substrate. Therefore, the model neglected any friction between the mold and substrate.

For stress analysis, the ice–substrate interface was assumed intact, and the experimentally measured ice detachment force was applied as an input to the model. In this way, the static stress distribution at the interface was obtained as an output. A custom APDL script extracted nodal stress values for a detailed analysis. For toughness calculations, a crack was introduced at the ice–substrate interface and incrementally advanced to simulate detachment, while simultaneously applying the experimentally measured force during crack propagation. The ice block was split into bonded and detached regions, with crack propagation modeled along a straight line perpendicular to the loading direction. Additional details on the interfacial toughness calculation method and mesh independence of the model can be found in the SI of ref. 54.

4.6 Stress and toughness correction factors

The framework introduced in ref. 41 and 54 employed a numerical model to derive the correction factors for the stress- and toughness-dominated interfacial fractures. Specifically, for stress-dominated fractures, a correction factor was used to account for stress concentrations at the interface and estimate the critical stress value, τ_c, which differed from the average shear stress ($\tau_{ave} = F/A$). Depending on the test system geometry, stress variations up to one order of magnitude could occur at the interface, which typically leads to an overestimation of τ_c, as previously shown in ref. 54.

In the case of toughness-dominated fractures, the direct measurement of the interfacial toughness using a mechanical push test can be challenging due to the influence of various factors, including the test system geometry and the elastic modulus of the ice. For this reason, correction factors were used to determine the toughness from the force required to propagate an interfacial crack and detach the ice.

Author contributions

Luca Stendardo: conceptualization, methodology, validation, formal analysis, investigation, writing – original draft, and visualization. Francesca Villa: investigation, methodology, and writing – original draft. Davide Parlato: investigation. Riccardo Motto: investigation. Mauro Mameli: conceptualization, funding acquisition, project administration, and writing – original draft. Carlo Antonini: conceptualization, methodology, formal analysis, writing – original draft, supervision, project administration, and funding acquisition. Paola Bassani: conceptualization, methodology, formal analysis, writing – original draft, supervision, project administration, and funding acquisition.

Conflicts of interest

There are no conflicts of interest to declare.

Data availability

All data generated or analyzed during this study are included in this published article and its supplementary information (SI). Supplementary information includes the 3D profilometer images (S1), dynamic contact angle data for NiTi samples (S2), stress–strain graphs for the tensile tests (S3), a description of the theoretical fracture mechanics framework (S4), data on ice detachment forces (S5), ice adhesion *vs.* roughness data (S6), SEM images (S7), a detailed analysis on surface roughness features (S8), and differential scanning calorimetry data (S9). See DOI: https://doi.org/10.1039/d5mh02106e.

Acknowledgements

This project has received funding from SMARTICE (Advanced de-icing surfaces based on engineered shape memory alloys, CUP: H53D23001840006) through the PRIN 2022, granted by the Italian Ministry of University and Research as part of Next Generation EU funding from the European Union. The authors thank Mr. Enrico Bassani for the preparation of the samples and for the technical assistance. The authors equally thank Dr. Carlo Alberto Biffi for the 3D optical microscopy images and extended roughness profiles. The authors also thank Mr. Jacopo Barat for his assistance during experimental testing. The authors are thankful to Dr. Irene Tagliaro for the fruitful discussion that led to this article.

References

1 I. Tagliaro, A. Cerpelloni, V.-M. Nikiforidis, R. Pillai and C. Antonini, On the Development of Icephobic Surfaces: Bridging Experiments and Simulations, in *The Surface Wettability Effect on Phase Change*, ed. M. Marengo and J. De Coninck, Springer International Publishing, Cham, 2022, pp. 235–272.
2 A. Dhyani, J. Wang, A. K. Halvey, B. Macdonald, G. Mehta and A. Tuteja, Design and applications of surfaces that control the accretion of matter, *Science*, 2021, **373**(6552), DOI: 10.1126/science.aba5010.
3 X. Tian, T. Verho and R. H. A. Ras, Moving superhydrophobic surfaces toward real-world applications, *Science*, 2016, **352**, 142.
4 C. Antonini, M. Innocenti, T. Horn, M. Marengo and A. Amirfazli, Understanding the effect of superhydrophobic coatings on energy reduction in anti-icing systems, *Cold Reg. Sci. Technol.*, 2011, **67**, 58.
5 *Smart Surface Design for Efficient Ice Protection and Control*, ed. C. Antonini and I. Tagliaro, IOP Publishing, 2025.
6 H. Zhang, *et al.*, Solar anti-icing surface with enhanced condensate self-removing at extreme environmental conditions, *Proc. Natl. Acad. Sci. U. S. A.*, 2021, **118**(18), DOI: 10.1073/pnas.2100978118.
7 Y. Zhuo, S. Xiao, A. Amirfazli, J. He and Z. Zhang, Polysiloxane as icephobic materials – The past, present and the future, *Chem. Eng. J.*, 2021, **405**, 127088.

8 G. Gastaldo, V. Pommier-Budinger and M. Budinger, Fracture Mechanisms in Electromechanical Resonant De-Icing Systems, in *Smart Surface Design for Efficient Ice Protection and Control*, ed. C. Antonini and I. Tagliaro, IOP Publishing, 2025, pp. 5-1–5-24.
9 D. L. Beemer, W. Wang and A. K. Kota, Durable gels with ultra-low adhesion to ice, *J. Mater. Chem. A*, 2016, **4**, 18253.
10 C. Wang, T. Fuller, W. Zhang and K. J. Wynne, Thickness Dependence of Ice Removal Stress for a Polydimethylsiloxane Nanocomposite: Sylgard 184, *Langmuir*, 2014, **30**, 12819.
11 P. F. I. Ibáñez, L. Stendardo, C. Ospina, R. Chaudhary, I. Tagliaro and C. Antonini, Discontinuity-enhanced icephobic surfaces for low ice adhesion, *J. Colloid Interface Sci.*, 2024, **403**(410), DOI: 10.1016/j.jcis.2024.09.205.
12 M. Fenero, M. Knez, I. Saric, M. Petravic, H. Grande and J. Palenzuela, Omniphobic Etched Aluminum Surfaces with Anti-Icing Ability, *Langmuir*, 2020, **36**, 10916.
13 W. Huang, J. Huang, Z. Guo and W. Liu, Icephobic/anti-icing properties of superhydrophobic surfaces, *Adv. Colloid Interface Sci.*, 2022, **304**, 102658.
14 R. Menini, Z. Ghalmi and M. Farzaneh, Highly resistant icephobic coatings on aluminum alloys, *Cold Reg. Sci. Technol.*, 2011, **65**, 65.
15 C. Antonini, A. Amirfazli and M. Marengo, Drop impact and wettability: From hydrophilic to superhydrophobic surfaces, *Phys. Fluids*, 2012, **24**(10), DOI: 10.1063/1.4757122.
16 T. Maitra, M. K. Tiwari, C. Antonini, P. Schoch, S. Jung, P. Eberle and D. Poulikakos, On the Nanoengineering of Superhydrophobic and Impalement Resistant Surface Textures below the Freezing Temperature, *Nano Lett.*, 2014, **14**, 172.
17 D. Khojasteh, M. Kazerooni, S. Salarian and R. Kamali, Droplet impact on superhydrophobic surfaces: A review of recent developments, *J. Ind. Eng. Chem.*, 2016, **42**, 1.
18 T. Maitra, S. Jung, M. E. Giger, V. Kandrical, T. Ruesch and D. Poulikakos, Superhydrophobicity *vs.* Ice Adhesion: The Quandary of Robust Icephobic Surface Design, *Adv. Mater. Interfaces*, 2015, **2**, 1500330.
19 J. Chen, J. Liu, M. He, K. Li, D. Cui, Q. Zhang, X. Zeng, Y. Zhang, J. Wang and Y. Song, Superhydrophobic surfaces cannot reduce ice adhesion, *Appl. Phys. Lett.*, 2012, **101**, 111603.
20 N. M. Sarkari, *et al.*, Experimental debate on the overlooked fundamental concepts in surface wetting and topography *vs.* ice adhesion strength relationships, *J. Colloid Interface Sci.*, 2024, S0021979724027164.
21 X. Wu, V. V. Silberschmidt, Z.-T. Hu and Z. Chen, When superhydrophobic coatings are icephobic: Role of surface topology, *Surf. Coat. Technol.*, 2019, **358**, 207.
22 E. Martin, T. Vandellos, D. Leguillon and N. Carrère, Initiation of edge debonding: coupled criterion *versus* cohesive zone model, *Int. J. Fract.*, 2016, **199**, 157.
23 D. Leguillon, Strength or toughness? A criterion for crack onset at a notch, *Eur. J. Mech. A/Solids*, 2002, **21**, 61.
24 L. Stendardo, I. Tagliaro, V. Pommier-Budinger, M. Budinger and C. Antonini, Conceptual Framework for Ice Adhesion Investigation on Surfaces, in *Smart Surface Design for Efficient Ice Protection and Control*, ed. C. Antonini and I. Tagliaro, IOP Publishing, 2025, pp. 3-1–3-22.
25 K. Golovin, A. Dhyani, M. D. Thouless and A. Tuteja, Low–interfacial toughness materials for effective large-scale deicing, *Science*, 2019, **364**, 371.
26 Z. Azimi Dijvejin, M. C. Jain, R. Kozak, M. H. Zarifi and K. Golovin, Smart low interfacial toughness coatings for on-demand de-icing without melting, *Nat. Commun.*, 2022, **13**, 5119.
27 G. Hernández Rodríguez, G. Gastaldo, L. Stendardo, Y. Rafik, J. Pothin, M. Budinger, C. Antonini, V. Pommier-Budinger and A. M. Coclite, Icephobic Gradient Polymer Coatings Coupled with Electromechanical De-icing Systems: A Promising Ice Repellent Hybrid System, *Adv. Eng. Mater.*, 2024, 2401532.
28 Y. Liu, The superelastic anisotropy in a NiTi shape memory alloy thin sheet, *Acta Mater.*, 2015, **95**, 411.
29 N. Sharma, K. Jangra and T. Raj, Applications of Nickel-Titanium Alloy, *J. Eng. Technol.*, 2015, **5**, 1.
30 M. H. Elahinia, M. Hashemi, M. Tabesh and S. B. Bhaduri, Manufacturing and processing of NiTi implants: A review, *Prog. Mater. Sci.*, 2012, **57**, 911.
31 M.-W. Han, M.-S. Kim and S.-H. Ahn, Shape memory textile composites with multi-mode actuations for soft morphing skins, *Composites, Part B*, 2020, **198**, 108170.
32 W.-K. Jung, S.-M. Lee, S.-H. Ahn and J. Park, Development and assessment of a knitted shape memory alloy-based multifunctional elbow brace, *J. Ind. Text.*, 2022, **51**, 1989S.
33 M. Kim, H. Lee, Y. Cho, J. K. Heo, Y. Quan, S. W. Lee, H. J. Pahk and S. Ahn, Surface Nanopatterned Shape Memory Alloy (SMA)-Based Photosensitive Artificial Muscle, *Adv. Opt. Mater.*, 2022, **10**, 2102024.
34 M. Kim, H. Lee and S. Ahn, Laser Controlled 65 Micrometer Long Microrobot Made of Ni-Ti Shape Memory Alloy, *Adv. Mater. Technol.*, 2019, **4**, 1900583.
35 H. Lee, M. Kim, G. Lee, C. Kim and S. Ahn, Shape Memory Alloy (SMA)-Based Microscale Actuators with 60% Deformation Rate and 1.6 kHz Actuation Speed, *Small*, 2018, **14**, 1801023.
36 J. M. Jani, M. Leary and A. Subic, Shape Memory Alloys in Automotive Applications, *Appl. Mech. Mater.*, 2014, **663**, 248.
37 O. Benafan, M. R. Moholt, M. Bass, J. H. Mabe, D. E. Nicholson and F. T. Calkins, Recent Advancements in Rotary Shape Memory Alloy Actuators for Aeronautics, *Shape Mem. Superelasticity*, 2019, **5**, 415.
38 P. Dubey, Durable anti-icing copper-based alloy coating grown by the HVOF method, *Colloids Surf., A*, 2025, **725**, 137730.
39 J. Gerardi, R. Ingram and R. Catarella, A Shape Memory Alloy Based De-Icing System for Aircraft, in *33rd Aerospace Sciences Meeting and Exhibit*, American Institute of Aeronautics and Astronautics, Reno, NV, U.S.A., 1995.
40 Z. Goraj, *An Overview of the Deicing and Anti-Icing Technologies with Prospects for the Future*, 2004, vol. 29.

41 L. Stendardo, G. Gastaldo, M. Budinger, V. Pommier-Budinger, I. Tagliaro, P. F. Ibáñez-Ibáñez and C. Antonini, Reframing ice adhesion mechanisms on a solid surface, *Appl. Surf. Sci.*, 2023, **641**, 158462.
42 I. Tagliaro, V. Radice, R. Nisticò and C. Antonini, Chitosan electrolyte hydrogel with low ice adhesion properties, *Colloids Surf., A*, 2024, **700**, 134695.
43 C. Ospina, P. F. Ibáñez-Ibáñez, I. Tagliaro, L. Stendardo, S. Tosatti and C. Antonini, Low ice adhesion on soft surfaces: Elasticity or lubrication effects?, *J. Colloid Interface Sci.*, 2025, **677**, 494.
44 *ASM Handbook. 1: Properties and Selection: Irons, Steels, and High-Performance Alloys*, in 8. print, ASM International, Materials Park, Ohio, 2007.
45 D.-D. Zhuang, S.-H. Zhang, H.-X. Liu and J. Chen, Cavitation erosion behavior and anti-cavitation erosion mechanism of NiTi alloys impacted by water jet, *Wear*, 2023, **518**, 204631.
46 X. Ma, F. Li, J. Cao, J. Li, H. Chen and C. Zhao, Vickers microhardness and microstructure relationship of Ti-6Al-4V alloy under cyclic forward-reverse torsion and monotonic torsion loading, *Mater. Des.*, 2017, **114**, 271.
47 J. Chandradass, T. Thirugnanasambandham, P. Jawahar and T. T. M. Kannan, Effect of silicon carbide and silicon carbide/alumina reinforced aluminum alloy (AA6061) metal matrix composite, *Mater. Today: Proc.*, 2021, **45**, 7147.
48 Z. He, Y. Zhuo, F. Wang, J. He and Z. Zhang, Design and preparation of icephobic PDMS-based coatings by introducing an aqueous lubricating layer and macro-crack initiators at the ice-substrate interface, *Prog. Org. Coat.*, 2020, **147**, 105737.
49 P. F. Ibáñez-Ibáñez, F. J. Montes Ruiz-Cabello, M. A. Cabrerizo-Vílchez and M. A. Rodríguez-Valverde, Ice adhesion of PDMS surfaces with balanced elastic and water-repellent properties, *J. Colloid Interface Sci.*, 2022, **608**, 792.
50 Y. Liu, L. Ma, W. Wang, A. K. Kota and H. Hu, An experimental study on soft PDMS materials for aircraft icing mitigation, *Appl. Surf. Sci.*, 2018, **447**, 599.
51 K. Nargatti and S. Ahankari, Advances in enhancing structural and functional fatigue resistance of superelastic NiTi shape memory alloy: A Review, *J. Intell. Mater. Syst. Struct.*, 2022, **33**, 503.
52 K. Alasvand Zarasvand, C. Pope, M. Mohseni, D. Orchard, C. Clark and K. Golovin, Metallic Plate Buckling As a Low Adhesion Mechanism for Durable and Scalable Icephobic Surface Design, *Adv. Mater. Interfaces*, 2022, **9**, 2101402.
53 E. R. Naimon, W. F. Weston and H. M. Ledbetter, Elastic properties of two titanium alloys at low temperatures, *Cryogenics*, 1974, **14**, 246.
54 L. Stendardo, G. Gastaldo, M. Budinger, I. Tagliaro, V. Pommier-Budinger and C. Antonini, Why the adhesion strength is not enough to assess ice adhesion on surfaces, *Appl. Surf. Sci.*, 2024, **672**, 160740.
55 Y. H. Yeong, A. Milionis, E. Loth, J. Sokhey and A. Lambourne, Atmospheric Ice Adhesion on Water-Repellent Coatings: Wetting and Surface Topology Effects, *Langmuir*, 2015, **31**, 13107.
56 V. Palanque, E. Villeneuve, M. Budinger, V. Pommier-Budinger and G. Momen, Cohesive strength and fracture toughness of atmospheric ice, *Cold Reg. Sci. Technol.*, 2022, **204**, 103679.
57 M. A. Pervier and D. W. Hammond, Measurement of the fracture energy in mode I of atmospheric ice accreted on different materials using a blister test, *Eng. Fract. Mech.*, 2019, **214**, 223.
58 G. Sivakumar and S. Sundararajan, The effect of surface roughness, stiffness, and size on ice adhesion, *Cold Reg. Sci. Technol.*, 2024, **225**, 104271.
59 H. Memon, J. Wang and X. Hou, Interdependence of Surface Roughness on Icephobic Performance: A Review, *Materials*, 2023, **16**, 4607.
60 V. Vercillo, S. Tonnicchia, J. Romano, A. García-Girón, A. I. Aguilar-Morales, S. Alamri, S. S. Dimov, T. Kunze, A. F. Lasagni and E. Bonaccurso, Design Rules for Laser-Treated Icephobic Metallic Surfaces for Aeronautic Applications, *Adv. Funct. Mater.*, 2020, **30**, 1910268.
61 M. Huré, P. Olivier and J. Garcia, Effect of Cassie-Baxter *versus* Wenzel states on ice adhesion: A fracture toughness approach, *Cold Reg. Sci. Technol.*, 2022, **194**, 103440.
62 P. Irajizad, A. Al-Bayati, B. Eslami, T. Shafquat, M. Nazari, P. Jafari, V. Kashyap, A. Masoudi, D. Araya and H. Ghasemi, Stress-localized durable icephobic surfaces, *Mater. Horiz.*, 2019, **6**, 758.
63 X. Jiang, Y. Lin, X. Xuan, Y. Zhuo, J. Wu, J. He, X. Du, Z. Zhang and T. Li, Stiffening surface lowers ice adhesion strength by stress concentration sites, *Colloids Surf., A*, 2023, **666**, 131334.
64 R. Akbari and C. Antonini, Contact angle measurements: From existing methods to an open-source tool, *Adv. Colloid Interface Sci.*, 2021, **294**, 102470.